Analysis of noise and dynamical effects in zero-IF self-oscillating mixers

M. Pontón[1], S. Sancho[2], A. Herrera[3], A. Suárez[4]
University of Cantabria, Spain
[1]mabel.ponton@unican.es, [2]sanchosm@unican.es, [3]herreraa@unican.es, [4]suareza@unican.es

***Abstract*—Zero-IF self-oscillating mixers (SOMs), based on injection locking, enable a compact direct frequency conversion and substantially mitigate the phase noise problem of heterodyne SOMs. Despite these advantages, their operation is complex and susceptible to exhibit a variety of dynamical effects. Here the need for an optimum selection of the operation point in the static injection-locked curve is demonstrated, as well as the inability of the oscillator to follow the variations of the input signal from a certain modulation frequency. Then a noise analysis of the down-converted signal is presented, based on a conversion-matrix formalism applied to a semi-analytical formulation.**

***Keywords*—injection-locking, noise analysis, envelope transient**

I. Introduction

The zero-IF self-oscillating mixers (SOMs) presented in [1]-[2] enable a direct frequency conversion that avoids the need for both an oscillator and a mixer. As a result, they reduce power consumption and size, of general interest for the implementation of compact transmitter and receivers, such as those used in RFID and sensor systems. Zero-IF SOMs are based on the injection locking of an oscillator by an RF signal, which substantially mitigates the phase noise problem of heterodyne SOMs. Zero-IF SOMs can be used under both amplitude and frequency modulations, and the demodulation can be easily carried out by amplifying the voltage drop in a resistor of the bias circuitry. Their interest and potential are demonstrated in the recent work [2], which presents a sourceless bank of zero-IF SOMs to receive and demodulate simultaneously different data streams.

Despite their demonstrated usefulness, the operation of modulated injection-locked oscillators is complex and susceptible at exhibiting a variety of dynamical effects. The work [3] presented an analysis of the boundaries between zero-IF and heterodyne SOM operation in terms of the input frequency and power, as well as an analysis of possible instantaneous unlocking under amplitude modulations. However, other distortion mechanisms associated with their oscillatory nature have not yet been investigated. Their knowledge and accurate prediction should allow an optimized design of these compact circuits to take advantage of their full potential.

Here we will demonstrate the need for a proper choice of the operation point in the static injection-locked curve to avoid a relevant distortion of the demodulated signal. The impact of the modulation frequency will also be analyzed, showing the inability of the oscillator to follow the variations of the input signal above a certain value of the modulation frequency. Then a noise analysis of the down-converted signal will be presented, based on a conversion-matrix formalism applied to a semi-analytical formulation of the injection-locked oscillator. Initially, an analytical study of a simple cubic-nonlinearity oscillator, enabling insight into the problem, will be carried out. Then, a FET-based oscillator at 800 MHz will be considered.

II. Dynamical effects at the modulation scale

The cubic-nonlinearity oscillator of Fig. 1 is injection locked with an independent source $g_{in}(t)$ of amplitude G_{in} and frequency ω_{in}. Limiting the analysis to DC and the fundamental frequency, it is described with the equations:

$$\begin{aligned} A(0)V_0 + B(0)I_0(V_0, V_1) &= 0, \\ A(\omega_{in})V_1 + B(\omega_{in})I_1(V_0, V_1) &= G_{in}e^{j\varphi} \end{aligned} \tag{1}$$

where V_0, V_1 and I_0, I_1 are the components at DC and ω_{in} of the voltage $v(t)$ and the current $i(t)$, V_1 is an amplitude and φ is the phase shift between $g_{in}(t)$ and $v(t)$. The frequency dependent functions are $A(\omega) = j\omega C(R + j\omega L) + 1$ and $B(\omega) = R + j\omega L$. Because the two equations are coupled, V_0 will vary with ω_{in}. One obtains a closed curve $V_0(f_{in})$, where $f_{in} = \omega_{in}/2\pi$, though only the stable lower section of this curve has been represented in Fig. 2(a) and (b).

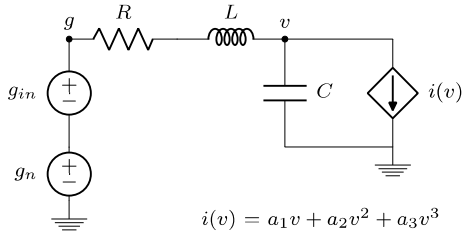

Fig. 1. Cubic-nonlinearity oscillator. The circuit parameter values are $a_1 = -0.2\ \Omega^{-1}$, $a_2 = 0.01$ A/V^2, $a_3 = 0.02$ A/V^3, $L = 0.1$ nH, $R = 0.1\ \Omega$, $C = 0.1$ nF. The injection source amplitude is $V_{in} = 0.02$ V.

When considering an input modulation, the state variables become time variant, and proceeding like in [4] one obtains:

$$\begin{aligned} &A(0)V_0(t) + B(0)I_0(t) - \\ &jA_\omega(0)\dot{V}_0(t) - jB_\omega(0)\dot{I}_0(t) = 0, \\ &A(\omega_{in})X_1(t) + B(\omega_{in})I_1(t) - \\ &jA_\omega(\omega_{in})\dot{X}_1(t) - jB_\omega(\omega_{in})\dot{I}_1(t) = G_{in}(t)e^{j\varphi(t)} \end{aligned} \tag{2}$$

where $X_1 = V_1 e^{j\phi(t)}$ and the subscript ω indicates frequency differentiation. As a meaningful example, we will consider an injection locking source at the free-running frequency $\omega_{in} = 2\pi f_o$, where $f_o = 1.583$ GHz is the free-running frequency,

and a frequency modulation $\Delta f_m(t) = A_m u(t, T_m)$, where $u(t, T_m)$ is a T_m periodic pulse taking values (0,1) in, $A_m = 4$ MHz and $f_m = 2\pi/T_m = 1$ MHz. Tracing the demodulated signal $V_0(t)$ versus the instantaneous frequency shift $\Delta f(t) = \dot{\phi}(t)/2\pi$, one obtains the black curve traced in Fig. 2(a), which exhibits a minimum. The instantaneous frequency and demodulated voltage $V_0(t)$ are traced versus time in Fig. 2(c) and (d) (blue curves). The demodulated voltage exhibits two maxima per period. This undesired effect is due to the minimum of the black curve in (a). Thus, a suitable choice of the operation point is required. For a higher modulation frequency $f_m = 10$ MHz one obtains the results in Fig. 2(b). Even though the modulation frequency excursion is the same as before, the projection over the static curve is smaller. This is because the oscillation is unable to follow the fast variations of the input signal [black waveforms in Fig. 2(c) and (d)], which is due to the impact of the time derivatives in (2).

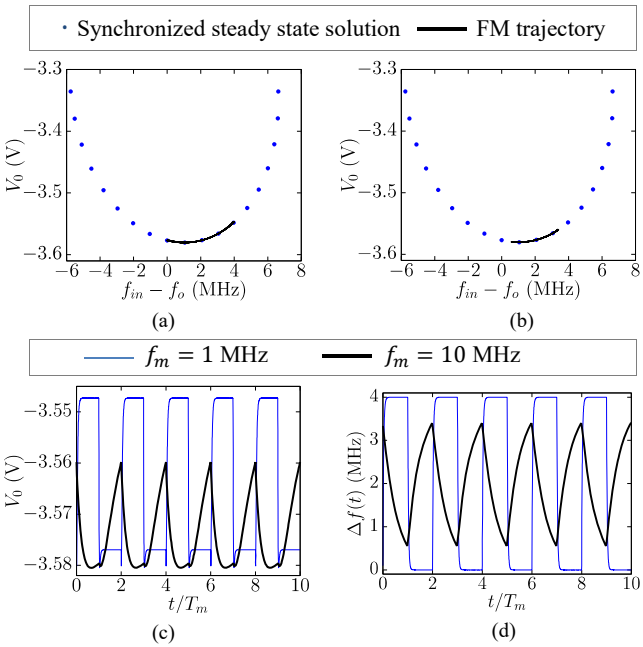

Fig. 2. FM analysis for $f_m = 1$ MHz, 10 MHz. (a) Evolution of the baseband signal $V_0(t)$ along the synchronization curve for $f_m = 1$ MHz. (b) For $f_m = 10$ MHz in (b). (c) Baseband signal $V_0(t)$ versus the normalized time t/T_m. (d) Instantaneous frequency shift $\Delta f(t)$ versus t/T_m.

Now a practical zero-IF SOM at 790 MHz shown in Fig. 3, based on the transistor ATF34143, will be considered. In view of the above results, the element values were optimized to avoid any extremes in the curve providing the DC signal versus ω_{in} (Fig. 4), obtained with harmonic balance (HB) [3]. The boundaries of the locking band are given by the turning-point bifurcations T_1 and T_2 [4], and the stable section is the lower one. A rectangular FM signal with amplitude $V_{in} = 0.07$ V and a frequency deviation of 4 MHz has been introduced, using different modulation frequencies: 1 MHz, 5 MHz, 10 MHz, and 15 MHz. The demodulated voltage has been traced versus the instantaneous frequency $f_{in} + \Delta f(t)$ (in red). The same curve (in red) is obtained for the four modulation frequencies, so the oscillation can follow the input signal in all cases.

The down-conversion gain depends on the device bias point. At a constant input frequency, this can be analyzed by sweeping the gate-bias voltage V_{GS} and performing an envelope-transient simulation at each sweep step. After removing the initial transient, the results are projected over the static injection-locked curve, and this projection gives rise to a vertical red line, for each V_{GS}. For $V_{in} = 0.07$ V and $f_m = 15$ MHz, one obtains the results in Fig. 5(a). As V_{GS} increases, there is a widening of the projection, which should imply a larger down-conversion gain. Note that near the turning point there is a qualitative change, due to the advance, in dynamic conditions, of the bifurcation that delimits the synchronization band. Fig. 5(b) and (c) compare the demodulated waveforms for $V_{GS1} = -0.258$ V and $V_{GS1} = -0.219$ V. As expected from Fig. 5(a), a higher gain is obtained for V_{GS2}. The two waveforms have been compared with the ones obtained experimentally with a simple bias tee.

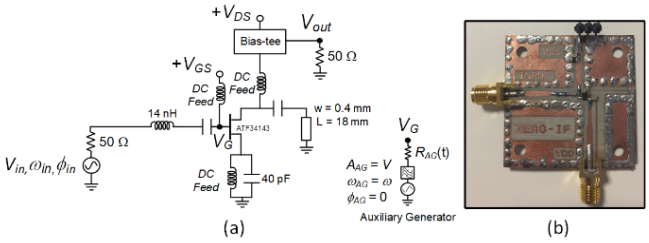

Fig. 3 Prototype on Rogers 4003C substrate. (a) Schematic. (b) Photograph.

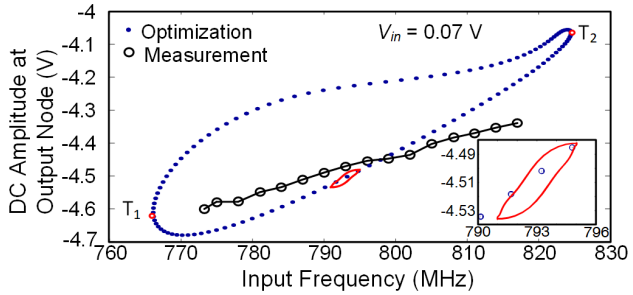

Fig. 4. Demodulated solution vs. the instantaneous frequency compared with the static curve obtained for $V_{in} = 0.07$ V. Measurements are superimposed.

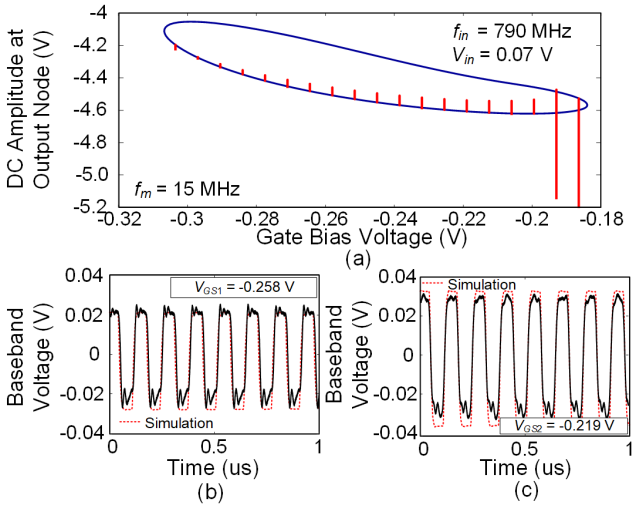

Fig. 5. FM demodulator. (a) Baseband amplitude at the output port versus the gate bias voltage for $V_{in} = 0.07$ V and $f_{in} = 790$ MHz. (b) and (c) Experimental validation of the FM demodulation (with $f_m = 15$ MHz) for two values of V_{GS}.

III. Noise Analysis

For an insightful noise analysis, we use a semi-analytical formulation, obtained by applying the Implicit Function Theorem (IFT) to the harmonic balance (HB) system [5]:

$$\begin{aligned} H_{-1}(V_0, V_1, \varphi, \omega) &\equiv Y(V_0, V_1, -\omega)V_1 - G_{in}e^{-j\varphi} = 0, \\ H_0(V_0, V_1, \omega)V_0 &\equiv G_0(V_0, V_1, \omega)V_0 = 0, \\ H_1(V_0, V_1, \varphi, \omega) &\equiv Y(V_0, V_1, \omega)V_1 - G_{in}e^{j\varphi} = 0 \end{aligned} \tag{3}$$

where Y is the total admittance function at ω and $-\omega$, and G_0 is the DC conductance and V_1 is the oscillation amplitude. System (3) can be compactly written as $\bar{H}(V_0, V_1, \varphi, \omega) = \bar{0}$. For a manageable analytical study, we will assume a small-frequency modulation $\Delta\omega_m(t)$, so the injection signal is:

$$\begin{aligned} g_{in}(t) &= 2Re\left\{G_{in}e^{j(\varphi+\Delta\varphi_m(t))}e^{j\omega_{in}t}\right\} \\ &\simeq 2Re\left\{(G_{in} + jV_{in}\Delta\varphi_m(t))e^{j(\omega_{in}t+\varphi)}\right\} \\ &= 2Re\left\{(G_{in}e^{j\varphi} + \Delta u(t))e^{j\omega_{in}t}\right\}, \end{aligned} \tag{4}$$

where $\Delta\varphi_m(t) = \int_0^t \Delta\omega_m(s)\,ds$. The modulation component

$$\Delta u(t) \equiv jV_{in}\Delta\varphi_m(t))e^{j\varphi} = \int_{-\infty}^{\infty} \Delta U(\Omega)e^{j\Omega t}d\Omega \tag{5}$$

fulfills $\Delta U(\Omega) = 0$ for $|\Omega| > \omega_b$ (modulation bandwidth). An equivalent noise source $g_n(t)$ with the components $\Delta N_k(\Omega)$, is also considered. Variables undergo the increments: $\Delta\bar{X}(\Omega) = (\Delta V_0(\Omega), \Delta V_1(\Omega), \Delta\varphi(\Omega))$ and the system becomes:

$$JH(V_0, V_1, \varphi, \omega + \Omega)\Delta\bar{X}(\Omega) = \Delta\bar{G}(\Omega) \tag{6}$$

where JH is the Jacobian matrix of $\bar{H}$ with respect to (V_0, V_1, φ) and the components of $\Delta\bar{G} = \Delta\bar{N}(\Omega) + \Delta\bar{U}(\Omega)$ are:

$$\begin{aligned} \Delta\bar{N}(\Omega) &= \left(\Delta N_{-1}(\Omega), \Delta N_0(\Omega), \Delta N_1(\Omega)\right)^t, \\ \Delta\bar{U}(\Omega) &= \left(\Delta U(-\Omega)^*, 0, \Delta U(\Omega)\right)^t \end{aligned} \tag{7}$$

The baseband perturbation $\Delta V_0(\Omega)$ can be expressed in terms of the noise and modulation components as:

$$\Delta V_0(\Omega) = \bar{Q}^+(\Omega, \varphi)(\Delta\bar{N}(\Omega) + \Delta\bar{U}(\Omega)) \tag{8}$$

where $\bar{Q}^+(\Omega, \varphi) = \left(Q_{-1}(\Omega, \varphi), Q_0(\Omega, \varphi), Q_1(\Omega, \varphi)\right)$ is a vector of sensitivity coefficients that depend on the phase shift φ. Note that $\Delta V_0(\Omega)$ is, in fact, an amplitude perturbation with the power spectral density (PSD):

$$\begin{aligned} \langle|\Delta V_0(\Omega, \varphi)|^2\rangle &= S_u(\Omega, \varphi) + S_n(\Omega, \varphi), \\ S_n(\Omega, \varphi) &= \sum_{k=-1}^{1} |Q_k(\Omega, \varphi)|^2\langle|\Delta N_k(\Omega)|^2\rangle, \\ S_u(\Omega, \varphi) &= |Q_{-1}(\Omega, \varphi)|^2\langle|\Delta U(-\Omega)|^2\rangle \\ &\quad + |Q_1(\Omega, \varphi)|^2\langle|\Delta U(\Omega)|^2\rangle \\ &\quad + 2Re\, Q_{-1}(\Omega, \varphi)^* Q_1(\Omega, \varphi)\langle\Delta U(-\Omega)\Delta U(\Omega)\rangle \end{aligned} \tag{9}$$

And the baseband signal to noise ratio is given by:

$$SNR_0(\varphi) = \frac{\int_{-\omega_b}^{\omega_b} S_u(\Omega)d\Omega}{\int_{-\omega_b}^{\omega_b} S_n(\Omega)d\Omega} \tag{10}$$

The analysis has been applied to the circuit in Fig. 3 at $f_{in} = 790$ MHz. For a sinusoidal FM input with amplitude $V_{in} = 0.07$ V, $f_m = 15$ MHz and frequency deviation of 4 MHz, equation (10) provides $SNR_0 = 25$ dB. Fig. 6(a) presents the variation of the three coefficients versus Ω: Q_0 (directly accounting for baseband noise) is dominant for all Ω, and, as expected, Q_1 and Q_{-1} are identical for low offset. The three coefficients exhibit a resonance effect at about 200 MHz due to the system poles since the coefficients are transfer functions. The baseband noise spectrum is also shown in Fig. 6(a) (right axis). Flicker noise is not considered to better appreciate the consistency with the sensitivity coefficients. Fig. 6(b) presents the measurements with an R&S FSWP8-Phase Noise Analyzer at three f_{in} values. Fig. 6(c) presents the analyzed and measured variation of the baseband noise versus f_{in} at a 100 kHz offset. The figure provides the variation of the baseband noise along the closed solution curve in Fig. 4.

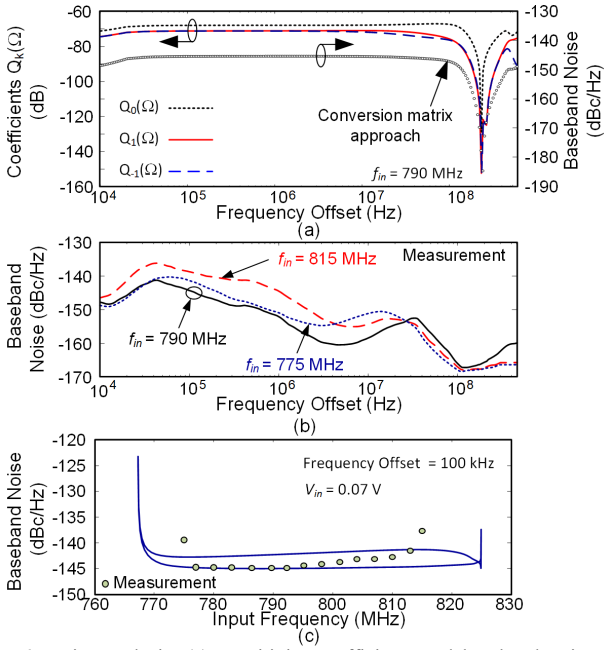

Fig. 6. Noise analysis. (a) Sensitivity coefficients and baseband noise. (b) Experimental measurements for three input frequencies. (c) Baseband noise versus f_{in} at 100 kHz offset (solid line) with measurements superimposed.

IV. Conclusion

The need for a suitable selection of the operation point of zero-IF frequency converters, avoiding any extremes of the static injection-locked curve, has been demonstrated. One must also take into account that beyond a certain modulation frequency, the oscillator instantaneous frequency is unable to follow the input signal. In a downconverter, the noise behavior is determined by the baseband noise spectral density.

Acknowledgement

Work supported by project TEC2017-88242-C3-(1/2)-R.

REFERENCES

[1] P. Burasa, N. G. Constantin and K. Wu , “Zero–IF Self–Oscillating Mixer for High Gbit/s Data–Rate Battery–Free Active uRFID Tag at Millimeter–Wave Frequencies in 65–nm CMOS," *IEEE Trans Microw. Theory Techn*., vol. 64, no. 4, pp. 1055–1065, 2016.

[2] P. Burasa, B. Mnasri and K. Wu, "Millimeter-Wave CMOS Sourceless Receiver Architecture for 5G-Served Ultra-Low-Power Sensing and Communication Systems," *IEEE Trans. Microw. Theory Tech.*, vol. 67, no. 5, pp. 1688-1696, May 2019.

[3] M. Pontón, A. Herrera, A. Suárez, "Double Functionality Concurrent Dual Band Self-Oscillationg Mixer," *IEEE Trans. Microw. Theory Tech,* (Early Access Article).

[4] E. Ngoya and R. Larcheveque, “Envelop transient analysis: A new method for the transient and steady state analysis of microwave communication circuits and systems,” *IEEE MTT-S Int. Microw. Symp. Dig.*, San Francisco, CA, USA, Jun. 1996, vol. 3, pp. 1365–1368.

[5] S. Sancho, S. Hernández and A. Suárez, "Noise Analysis of Super-Regenerative Oscillators in Linear and Nonlinear Modes," *IEEE Trans. Microw. Theory Tech*, vol. 67, no. 12, pp. 4955-4965, Dec. 2019.